

# Numerical study on airflow performance and mechanical characteristics of centrifugal fan

Minkai Bai<sup>1</sup>, Haihui Tan<sup>2</sup>, and Zhan Liu<sup>1\*</sup>

<sup>1</sup>School of Mechanic and Civil Engineering, China University of Mining and Technology, Xuzhou, China

<sup>2</sup>School of Mechanical and Electrical Engineering, University of Electronic Science and Technology of China, Zhongshan Institute, Zhongshan, China

**Abstract.** As small fans are widely used to dissipate the heat of the electronic components, a series of special requirements are put forward on the airflow performance and stress characteristics. In the present study, the computational fluid dynamics (CFD) method is adopted to study the airflow characteristics of a specific type of fan, including the fluid pressure distribution, flow velocity field and fluid streamline distribution. The stress characteristics of the fan blades are systematically analyzed based on the fluid-solid coupling and thermal-solid coupling methods. The results show that with the rotation speed of 1400 rpm, the airflow velocity in the air duct is unevenly distributed, and some eddy disturbances form and occur in the flow field. To improve the operating efficiency of the fan, appropriate optimization schemes should be adopted to reduce the intensity and range of the eddy influence. When the inlet temperature is 20 °C, the stress on the impeller is mainly caused by centrifugal force and thermal load. As the inlet temperature increases, the effect of the thermal load becomes increasing. While for the centrifugal force, its influence on the impeller gradually disappears and completely disappears when the temperature reaches 50 °C.

## 1 Introduction

Fans are widely used in industrial and civil engineering as ventilation and dust removal equipment[1]. With the development of electrical equipment, fans are utilized to enhance heat dissipation[2] generated by computers and refrigerators. Different application scenarios put a series of requirements on the flow field and operation performance of fans[3, 4]. Until now, more investigations were conducted on the performance of fans in different cooling scenarios. Yamam et al.[5] analyzed the performance of fans in electronic cooling by numerical simulations and evaluated the accuracy of the numerical simulations. Guo et al.[6] numerically researched the flow field of a high-voltage fan on fuel cell vehicles and obtained the optimal layout strategy of the dual fan system.

The flow field inside the casing is a complex three-dimensional strong cyclonic flow with highly nonlinear characteristics. During the high-speed rotation of the fan, the impeller is subjected to centrifugal force, the aerodynamic force caused by the flowing air and the thermal load in some heat dissipation scenarios[7]. When fans are constantly operated at high rpm, both the noise generated by the fan and the impact on the impeller become obvious and serious[8]. As the requirements for the various parameters of the fan become increasingly high, the stress study on fan impellers has become of great interest. Glessner[9] adopted analytical techniques to predict the determination of stresses in the fan impeller. Zhu[10] researched the stress distribution and

deformation on the impeller with the three-dimensional finite element method. However, with increasing of the heat dissipation requirement, the effect of temperature on the impeller stress becomes increasingly evident. Zheng[11] used a solid-fluid coupled method to analyze the effects of temperature and pressure on the stresses of the impeller with different inlet conditions.

In this study, a three-dimensional numerical simulation is conducted on a specific model of the fan. The velocity and pressure fields are simulated, and the flow patterns within the fan are analyzed. As the impeller material of the fan studied in this paper is plastic, which is influenced by temperature in some heat dissipation scenarios, the force characteristics and deformation of the fan impeller at different temperatures are considered and researched. The fluid-solid coupling and thermal-solid coupling methods are adopted to simulate the force characteristic of the fan impeller. With the deformation and stress distribution of the fan impeller obtained, the reliability of the fan is evaluated. The present study is significant to the optimal design of the fan.

## 2 Numerical simulation

### 2.1 Physical model

The centrifugal fan, as shown in Fig. 1, mainly consists of the impeller, hub and shell. The rotation speed of the fan is 1400 r/min.

\* Corresponding author: [liuzhankd@cumt.edu.cn](mailto:liuzhankd@cumt.edu.cn)

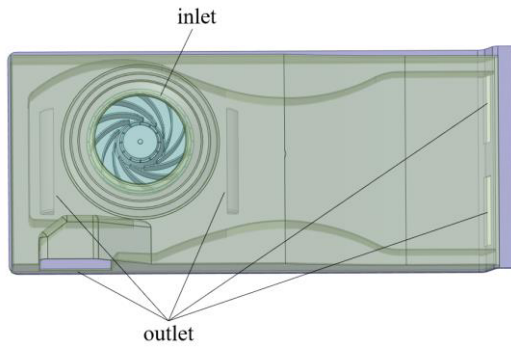


**Fig.1.** Physical model of fan

### 2.2 Model calculation methods and boundary conditions

In this paper, the commercial Fluent software is used to simulate the fluid flow within the fan. The Multiple Reference Frame (MRF) model is utilized to calculate the coupling relationship between the rotation domains and the adjacent flow domains in steady-state. The rotational coordinate system is adopted in the rotating region, while the entrance and exit regions are relatively static. The inlet and outlet of airflow are set as pressure ports, and the initial gauge pressure is set to 0 Pa. That is to say, there was no additional pressure effect. The fan blade is defined as a rotating wall, the shell part is set with stationary boundary conditions, and the standard wall function is set in the near-wall region. The Static Structure and Steady-State Thermal are used to carry out fluid-structure and thermal-solid coupling of the model to analyze the stress and deformation of the impeller. Ye[12] verified the feasibility of this model by comparing the simulation results with the experimental results. This paper simulates the  $k-\omega$  model and  $k-\epsilon$  model separately and finds that they have similar simulation results, but  $k-\omega$  has better convergence. Finally, the SST  $k-\omega$  turbulence model is used for the steady-state simulation of the fan model.

### 2.3 Mesh generation

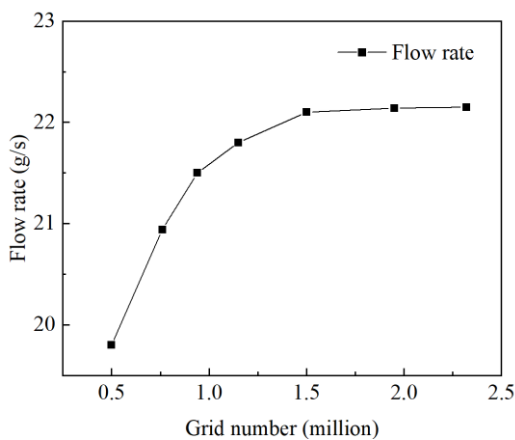


**Fig. 2.** Grid independence verification

Based on the complex geometric structure, the calculation mesh is generated by using a polyhedral type element and the methods of local encryption are used to improve the

mesh quality[13]. The numerical model can be divided into non-rotating and rotating regions according to different motion characteristics. The rotation area is divided into dense grids and the non-rotating region with sparse grids. To verify the accuracy of the mesh, the mesh independence analysis is conducted. As Fig. 2 shows, when the grid number exceeds 1.5 million, the flow rate at the fan inlet has small variations. Therefore, the final grid number of the model is determined to be 1.55 million.

## 3 Results and discussion

### 3.1 Flow field analysis

Driven by the rotating impeller, air firstly enters the fan along the axial direction of the impeller, then flows toward different outlets. During this process, the air obtains certain momentum under the continuing compression by the rotating impeller. The static pressure and velocity vector distribution for the middle section of the fan are shown in Fig. 3. As Fig. 3(a) shows, the pressure at the inlet of the impeller is very low, and the external environment air can be inhaled. At the outlet of the impeller, the air has a high velocity and a low pressure. Once thrown from the impeller, the air velocity decreases and the pressure increases gradually. Some fluid-flow phenomena within turbomachinery, such as typical unsteady and rotating flow phenomena, are shown schematically in Fig. 3(b). It can be seen that in the throat of the runner, the velocity-pressure distribution of the airflow is more chaotic, and there are two regions with great disturbances. Disturbance zone 1 takes shape between two faster flow regions, which is disturbed due to the velocity difference between higher and lower velocity fluids. An anticlockwise vortex forms in disturbance zone 2. The vortex is caused by the split effect of the side outlet, with a low flow rate and high pressure.

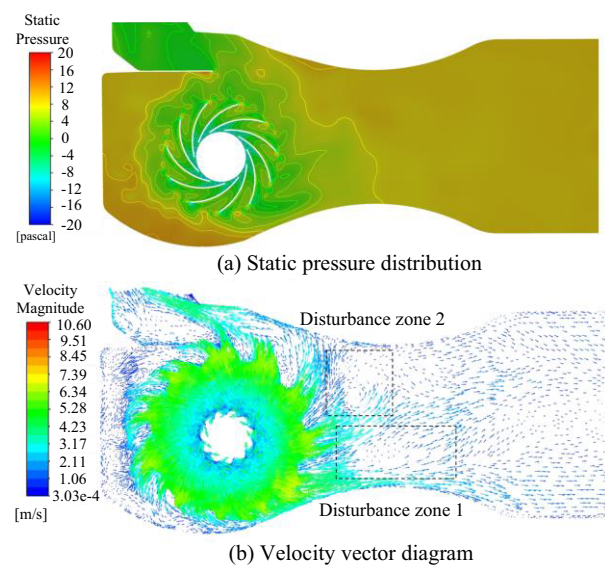


**Fig. 3.** Static pressure distribution and velocity vector diagram

These phenomena produce fluid rotation, which appears as secondary, smaller scale, dissipative fluid motions, which may severely distort the flow field and

cause significant power losses in fans. Therefore, it is necessary to reduce the disturbances in practical cases. The shape of the duct and the position of the outlet cause obvious influences on the fluid flow. Adjusting the runner is the main direction of optimizing the model. For this model, the throat cross-sectional area can be reduced to merge the two high-velocity regions to reduce the velocity difference. The position of the outlet side runner can be also adjusted to reduce the disturbance caused by the split flow to avoid the creation of the vortex.

### 3.2 Stress analysis of fan impeller

The impeller is made of PBT. The material properties of the impeller are shown in Table 1.

**Table 1** The main characteristic parameters of the impeller

Parameter	Elastic Modulus	Poisson's ratio
Value	1930 N/mm <sup>2</sup>	0.398

The working revolution is set as 1400 r/min and the rotation direction is clockwise around the impeller axis. The inlet temperature is set as 20 °C and the influence of the gravity is neglected. It can be seen from Fig. 4(a) and (b) that the equivalent stresses of the impeller under centrifugal force and aerodynamic force have the same trend. The maximum stress occurs on the contacted position of the blade and the hub, and the minimum stress occurs on the hub. As Fig. 4(c) shows, under the thermal load, the equivalent force is concentrated on the hub. Moreover, the centrifugal force and aerodynamic force have similar effects on the stress distribution on the blade. The blade has large stress around the contact position with the disc and the stiffening ring. The stress at the center of the blade is relatively small. For the blade stress distribution caused by the thermal load, large stress occurs on the contact position with the disc and the stress decreases with the increase of the distance from the contact surface.

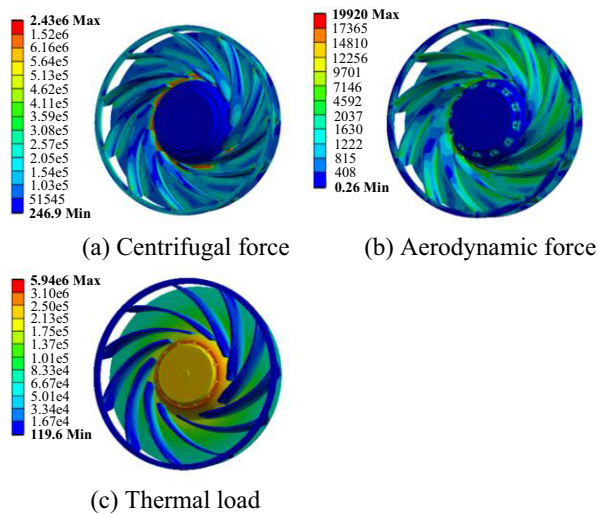


**Fig. 4.** Stress distribution of the impeller under different loads

By comparing Fig. 4 (a) and (c), it can be seen that the stress caused by centrifugal force mainly appears in the blade and the thermal stress mainly occurs on the hub. Therefore, at the operating temperature of 20 °C, the

stress distribution on the blade is mainly influenced by the centrifugal force. The stress caused by centrifugal force, aerodynamic force, and thermal load are  $1.039 \times 10^5$  Pa,  $1.027 \times 10^3$  Pa, and  $1.96 \times 10^5$  Pa, respectively. It can be found that the stress on the impeller is mainly caused by centrifugal force and thermal load and is less influenced by aerodynamic force. Thermal stress accounts for >50% of the total stress when the inlet temperature is 20 °C, which means that the temperature must be considered for analyzing the stress of the impeller.

The maximum stress on the impeller is 4.03 MPa, while the impeller's yield stress is 58.2 MPa. Hence the strength of the impeller meets the requirement. Combined Fig. 5 (a) and Fig. 4 (a), it is clear to see that the stress distribution on the blade under total load is similar to that of the blade under the centrifugal force, which further indicates that the stress distribution on the blade is mainly influenced by centrifugal force. The total displacement distribution of the impeller in cylindrical coordination is shown in Fig. 5. The maximum deformation of the impeller occurs on the tip of the blade, with a value of  $2.13 \times 10^{-5}$  m. While the minimum deformation occurs on the hub and the average deformation is  $1.14 \times 10^{-5}$  m. It is worth noting that the deformations caused by centrifugal force and thermal load are  $1.21 \times 10^{-5}$  m and  $1.52 \times 10^{-5}$  m, which are larger than the deformation under the total load. The results show that the centrifugal force and the thermal load act on the impeller in different bending moment directions, even in the opposite direction. Therefore, with the increase of load, the deformation of the impeller is not simply superimposed, but also decreases due to the mutual restraint of load.

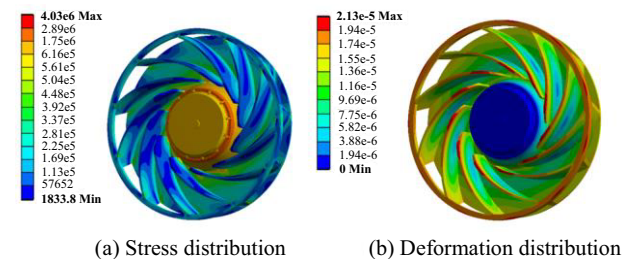


**Fig. 5.** Stress distribution and deformation of the impeller under total load

It can be seen from Fig. 6 (a), (c) and (e) that with the inlet temperature of 30 °C, the thermal stress on the blade is concentrated at the bottom of the blade. The influence range of the thermal load expands with the increase of the inlet temperature. When the inlet temperature reaches 50 °C, it eventually covers almost the entire blade. As shown in Fig 6 (b), (d) and (f), when the inlet temperature is 30 °C, the stress on the impeller is mainly caused by the thermal load. Meanwhile, the action characteristic of centrifugal force (larger stresses around the contact points with the hub and stiffening ring) is also imposed on the blade. However, as the temperature increases, the centrifugal force characteristic gradually disappears and almost completely disappears when the inlet temperature reaches 50 °C. Correspondingly, the thermal load gradually tends to play the dominant role. As Fig. 7 shows, with the increase of the temperature, the magnitude of the thermal stress is close to the magnitude of the total stress.



When the inlet temperature is 50 °C, the two magnitudes are almost identical. This means that the effect of other loads on the impeller can be neglected. It is worth mentioning that when the inlet temperature is 50 °C, the maximum stress in the impeller reaches 50.6 MPa, which is quite close to the yield stress. Therefore, to ensure the normal operation of the fan, it is necessary to ensure that the inlet temperature is below 50 °C.

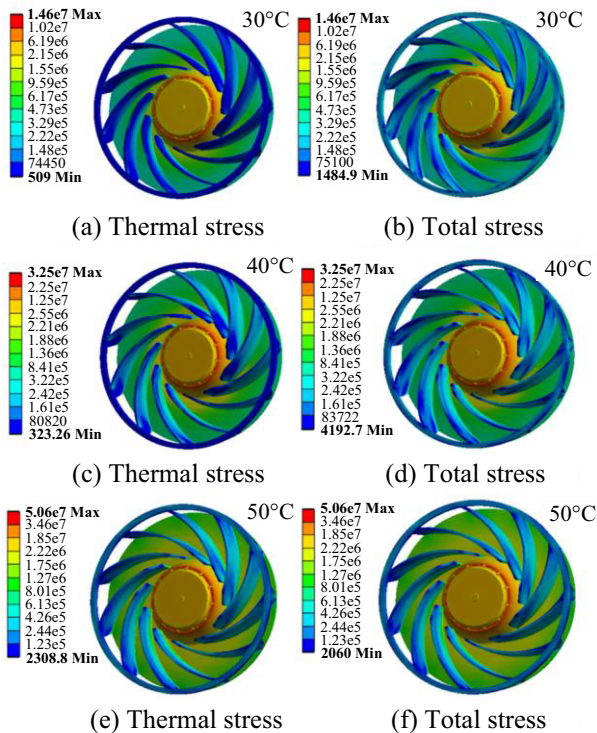


**Fig.6.** Stress distribution of the impeller at different temperatures

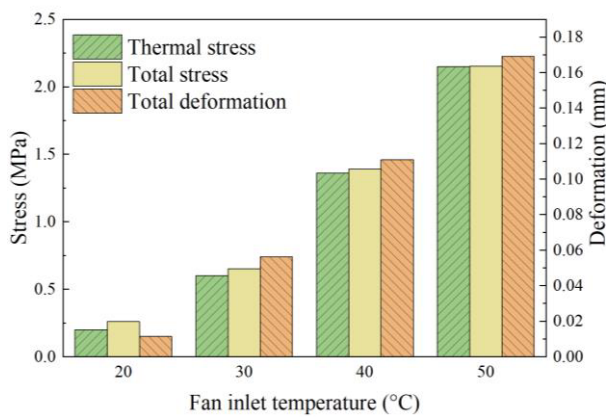


**Fig. 7.** Average stress and deformation of the impeller at different temperatures

## 4 Conclusions

(1) In the fan flow channel, the disturbance or even vortex forms and causes momentum dissipation. The flow channel must be properly adjusted to minimize interference.

(2) When the inlet temperature is 20 °C, the stress on the impeller is mainly caused by centrifugal force and thermal load, and is less influenced by aerodynamic force. With

the increase of the load, the deformation of the impeller is not only simply superimposed but also decreased due to the mutual restraint of the loads.

(3) With the increase in temperature, the thermal load gradually dominates and the influence of centrifugal force on the impeller gradually disappears. When the inlet temperature reaches 50°C, other loads can be completely neglected and the maximum stress of the impeller is close to the yield limit. To ensure the safety operation performance, the operating temperature of the fan must be below 50 °C.

## References

1. [W. Choi, M.B. Pate, and J.F. Sweeney, \*Study of bathroom ventilation fan performance trends for years 2005 to 2013—Data analysis of loudness and efficacy.\* Energy Build., \*\*116\*\*: p. 468-477\(2016\).](#)
2. [J. Stafford, E. Walsh, and V. Egan, \*A study on the flow field and local heat transfer performance due to geometric scaling of centrifugal fans.\* Int J Heat Fluid Flow, \*\*32\*\*\(6\): p. 1160-1172\(2011\).](#)
3. [S.-C. Lin and M.-L. Tsai, \*An integrated performance analysis for a backward-inclined centrifugal fan.\* Comput Fluids, \*\*56\*\*: p. 24-38\(2012\).](#)
4. [C.X. Li, S.L. Wang, and Y.K. Jia, \*The performance of a centrifugal fan with enlarged impeller.\* Energy Convers. Manag., \*\*52\*\*\(8-9\): p. 2902-2910\(2011\).](#)
5. [Y.M. Manaserh, et al., \*Degradation of Fan Performance in Cooling Electronics: Experimental Investigation and Evaluating Numerical Techniques.\* Int. J. Heat Mass Transf., \*\*174\*\*\(2021\).](#)
6. [R. Guo, et al., \*Research on aerodynamic performance and noise reduction of high-voltage fans on fuel cell vehicles.\* Appl Acoust, \*\*186\*\*\(2022\).](#)
7. [T.R. Jebieshia, S.K. Raman, and H.D. Kim, \*Aerodynamic and Structural Characteristics of a Centrifugal Compressor Impeller.\* Appl. Sci., \*\*9\*\*\(16\)\(2019\).](#)
8. [D.V. Bhope and P.M. Padole, \*Experimental and theoretical analysis of stresses, noise and flow in centrifugal fan impeller.\* Mech Mach Theory, \*\*39\*\*\(12\): p. 1257-1271\(2004\).](#)
9. [J. Glessner, \*A method for analyzing stresses in centrifugal impellers.\* ASME, \(54-A\): p. 167\(1954\).](#)
10. [L.D. Zhu, et al., \*Statics Analysis of Integral Impeller Based on Finite Element.\* Adv Mat Res, \*\*753-755\*\*: p. 1124-1127\(2013\).](#)
11. [X.Q. Zheng and C. Ding, \*Effect of temperature and pressure on stress of impeller in axial-centrifugal combined compressor.\* Adv. Mech. Eng., \*\*8\*\*\(6\)\(2016\).](#)
12. [X. Ye, et al., \*Numerical investigation of blade tip grooving effect on performance and dynamics of an axial flow fan.\* Energy, \*\*82\*\*: p. 556-569\(2015\).](#)
13. [X. Liu, et al., \*Experimental and numerical simulation investigations of an axial flow fan performance in high-altitude environments.\* Energy, \*\*234\*\*\(2021\).](#)